RSC Advances

PAPER

View Article Online
View Journal | View Issue

Cite this: *RSC Adv.*, 2025, **15**, 29646

Phosphorous waterborne polyurethanes/single-walled carbon nanotube composites as flame retardant building materials and their application in architectural design

Junyu Pan * and Yang Zhong

Development of building materials with high flame retardancy and electromagnetic interference (EMI) shielding is an urgent issue. Given the superior advantages of single-walled carbon nanotubes (SWCNTs) including excellent thermal/electric conductivity and low percolation threshold as fillers, novel phosphorous/SWCNTs/waterborne polyurethanes (P/SWCNTs/WPUs) were fabricated by an *in situ* polymerization, in which SWCNTs with small bundle (8.32 nm of average diameter) were prepared *via* a floating catalyst chemical vapor deposition. Multiple characterization results including composite morphology, increasing ratio of emerging covalently bonding of nitrogen/phosphorous revealed the successful phosphorous-containing composite of P in matrix. Composite with 15 wt% SWCNTs exhibited excellent flame retardant including 4.6 cm of damage length and 34.1% of limiting oxygen index without obvious destroy of original morphology. Superior electrical conductivity (4.52 S cm^{-1}) and EMI shielding (21.8 dB) were exhibited. More obvious rising trend of reflection values (4.6–19.3 dB) than that of absorption values (4.9–9.6 dB) indicated that the improvement of reflection derived from the conductivity enhancement with higher SWCNT content. Moreover, an excellent EMI shielding durability with 1.8% of reduce was achieved after 1000 times of bending. The applications of P/SWCNTs/WPUs in the building design for walls were discussed. This study provided a new insight in the usage of SWCNTs in flame retardant and EMI polymers.

Received 25th July 2025
Accepted 15th August 2025

DOI: 10.1039/d5ra05374a

rsc.li/rsc-advances

1 Introduction

High-speed development of electronic information, electronic and electrical equipment in multiple fields provides great benefits for daily life as well as exposes serious electromagnetic pollution problems.[1–3] In view of the increasingly serious electromagnetic pollution, electromagnetic interference (EMI) shielding materials including metal conductor, ferromagnetic materials, surface conductive materials and polymers have been developed.[4,5] Among them, polymer EMI materials have the advantages of good plasticity, easy processing, light weight, stable performance, wide application range and low cost, which can satisfy the requirements of "thin, light, flexible and strong" for advanced novel EMI materials. In the fifth generation mobile communication network, communication devices with large capacity and high speed transmission induce the significant increase of electromagnetic radiation and power consumption. The heat dissipation caused by the increasing power consumption would even lead to the fire of electronic components.[6,7] Due to the flammability of polymers, it is easy to cause fire accidents of polymers in the actual high-power electromagnetic application. Therefore, it is highly desirable to develop polymer EMI shielding materials with high fire safety.

Polyurethane (PU) is a multifunctional organic polymer material with excellent properties including good mechanical properties, low density, light weight, good thermal insulation performance and easy installation. PU has been widely used in the construction field.[8–11] Introduction of PU foam into building constructions not only reduces the usage of traditional building materials, but also greatly shortens the construction period because of its easy installation and construction. PU with good thermal insulation performance reduces the energy consumption of building heating and cooling. The application of PU materials in the field of architecture has improved the living experience obviously. Waterborne polyurethane (WPU), as a new environment-friendly coating material, is different from the traditional organic solvent-based polyurethane coating.[12–14] WPU takes water as the solvent and presents multiple characteristics of PU, such as wide hardness, abrasion resistance, high strength and high adhesion.[15] Meanwhile, WPU is of low volatile organic compounds and no hazardous air pollutants, which has been commonly applied as building materials due to its

Art, Design & Architecture, University of New South Wales, Sydney 2000, Australia. E-mail: junyu_pan2025@163.com

advantages in the environmental protection and inexpensive price.[16]

Moreover, functional nanomaterial-filled polymer materials exhibited promising EMI performances properties, becoming a more promising alternative filling material for EMI shielding.[17] Since EMI property of polymers is derived from fillers, carbonaceous materials including graphene, carbon nanotubes (CNTs) and their composites have stood out.[18–23] Introducing carbon-based fillers with high conductivity is considered as a promising strategy to improve the conductivity and EMI shielding of composites. Among these carbonaceous materials, single-walled carbon nanotubes (SWCNTs) presented electrical conductivity, high aspect ratio and low density.[24–28] Therefore, SWCNTs have been added in polymer matrix as conductive fillers. Compared with multiple-walled CNTs (MWCNTs)-filled EMI polymers, there is a scarcity of reports on the latest development in applying SWCNTs-based coating materials with high electrical conductivity in the management of EMI. Furthermore, CNTs offer an alternative solution for flame retardant polymeric materials. For instance, polyelectrolyte amino-modified MWCNTs and ammonium polyphosphate (APP) were combined into ramie fabrics, showing an obviously enhanced flame retardant.[29] Amine MWCNTs could achieved the same performance with 100 times lower filling content compared to traditional flame retardants.[30] Compared with MWCNTs-filled flame retardant polymers, few studies for SWCNTs-based flame retardant polymers have been presented.

In this work, SWCNTs was prepared using a floating catalyst chemical vapor deposition (FCCVD). A novel fire-resistant and EMI shielding WPU was fabricated by combining SWCNTs and APP through an *in situ* polymerization method. The morphology, thermal behavior, flame retardancy, electrical conductivity and EMI shielding of phosphorous/SWCNTs/WPU composites (P/SWCNTs/WPUs) with various contents of SWCNTs were investigated.

2 Experimental

2.1. Materials

APP, dimethylol butanoic acid (DMBA), isophorone diisocyanate (IPDI), ethylenediamine (EDA), triethylamine (TEA), acetone and polycaprolactone diol (PCL diol, and average M_n = 10 000) were of analytical grade and purchased from Sigma-Aldrich Co., Ltd.

2.2. Fabrication of P/SWCNTs/WPU coatings

2.2.1 SWCNTs fabrication. FCCVD method was applied to fabricate SWCNTs. Specifically, liquid carbon source (*i.e.*, toluene), catalyst precursor (*i.e.*, ferrocene) and growth promoter (*i.e.*, thiophene) were added to the reaction zone of FCCVD furnace at 1100 °C with the flowing of gaseous carbon source (*i.e.*, ethylene) and carrier gas (*i.e.*, hydrogen). The cracked carbon source was nucleated under the interaction with catalyst and growth promoter. The schematic diagram of experimental device for preparing SWCNTs by FCCVD was illustrated in Fig. 1. The main component was a vertical tube

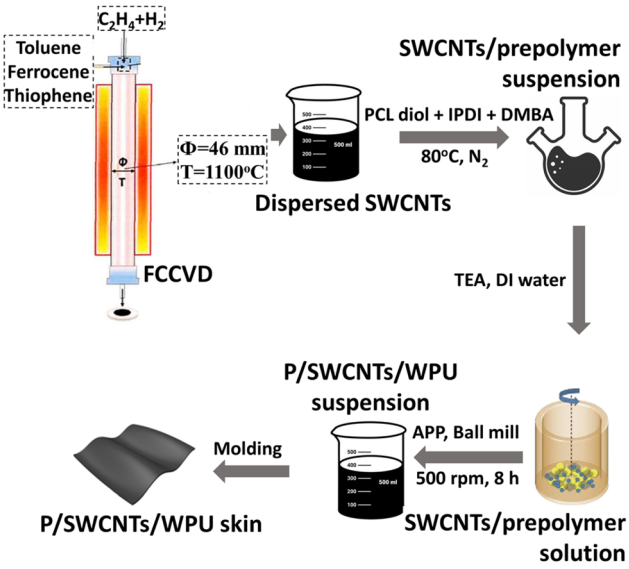

Fig. 1 Schematic illustration for the preparation of P/SWCNTs/WPU coatings.

furnace heated by resistance wire, in which the inner diameter of quartz tube reactor was 46 mm and the length was 1500 mm. There was an air inlet and a catalyst precursor injection port above the reaction furnace. Produced SWCNTs was carried by carrier gas to the film collection device below the reaction furnace, and SWCNT powder was obtained by the filtration with microporous membrane.

2.2.2 Fabrication of P/SWCNTs/WPU coatings. Homogeneous SWCNT dispersion with different SWCNT weights were prepared. With a continuous stirring at 80 °C under nitrogen atmosphere, 7.7 g PCL diol, 3.4 g IPDI and 0.6 g DMBA were added to prepare SWCNTs/polyurethane. Afterward, 3.0 g EDA and APP (1.0 wt%) solution were added to SWCNTs/prepolymer suspension before a ball mill treatment (400 rpm and 12 hours). Then, P/SWCNTs/WPUs was obtained named as P/SWCNTs/WPU-*x*, where *x* is the sequence (*i.e.*, 1, 2, 3 and 4) of SWCNT mass content in composites (*i.e.*, 5 wt%, 10 wt%, 15 wt% and 20 wt%).

2.3. Characterization and measurements

Scanning electron microscopy (SEM) and transmission electron microscopy were used to observe the morphology of samples. Model of SEM used was Nova NanoSEM 430 with the accelerating voltage of 0.2–30 kV. Sample for SEM analyzed was prepared by attaching SWCNTs to conductive tape and transferring it to silicon wafer for observation. Model of TEM used was Tecnai F20 with the accelerating voltage of 300 kV, the point resolution of 0.20 nm, and the line resolution of 0.10 nm. Multi-wavelength Raman spectroscopy was used to analyze the diameter, mass and other structural information of SWCNTs. The model of Raman equipment used was Jobin-Yvon labram HR 800 with 1 μm^2 of spot size, <2 mW μm^{-2} of laser intensity and three excitable laser wavelengths including 532 nm, 633 nm and 785 nm. X-ray photoelectron spectroscopy (XPS) used was

ESCALAB 250 photoelectron spectrometer with Ka ray of monochromatic Al as radiation source. After the samples were tested, the binding energy of obtained elements was calibrated by C 1s binding energy (284.6 eV). Thermal property was evaluated under N_2 with 8 °C min^{-1} of heating speed at 80–800 °C. Fourier transform infrared spectra (FTIR) were recorded on Nicolet 6700 (Thermo Fisher Scientific Co. Ltd., USA) with the KBr disks in the wavenumber range of 4000–400 cm^{-1}. The standard of GB/T 5455-2014 was applied to guide the vertical flame tests. Specifically, methane flame was utilized to samples on one side for 20 s. The damage length was recorded using a camera. The standard of GB/T 5454 was applied to guide the oxygen index meter (5901A, VOUCH, China). The mixture of nitrogen and oxygen was utilized to burn samples and the limiting oxygen index (LOI) was calculated.

The thermal conductivity values (λ(W mK^{-1})) of samples were measured using a laser flash approach (LFA 467, Netzsch) as the following equation of $\lambda = \alpha \times C_p \times \rho$, where α was the thermal diffusivity (mm^2 s^{-1}), C_p was the specific heat capacity (J g^{-1} K^{-1}) and ρ was the density (g cm^{-3}) of samples. Mechanical property was measured *via* uniaxial tensile test with an Instron 5965 tester (Instron, Massachusetts, USA) at a velocity of 1 mm min^{-1}. Water contact angle of samples was measured *via* a contact angle meter (Theta Flex, Biolin Scientific).

3 Results and discussion

3.1. SWCNTs characterization

As shown in Fig. 2, SWCNTs prepared by FFCVD presented a clear and uniform morphology which was constructed by disordered net structure. No impurity particles such as catalyst particles or agglomerated particles were observed. Two typical morphologies of SWCNTs prepared by FFCVD were observed in TEM image, including single SWCNT and small bundle of SWCNTs. Diameter distribution of 280 SWCNTs was statistically analyzed as shown in Fig. 2c. ~38% of tubes was single SWCNT, and ~62% of tubes was SWCNT bundles with an average diameter of 8.32 nm. The diameter of SWCNTs with single morphology was large between 1.7 nm and 3.0 nm, and the tube wall was straight, which indicated that SWCNTs prepared by FCCVD had a high crystallinity. The controllable preparation of SWCNTs with high quality and small bundle of tubes was mainly attributed to the addition of hydrogen with large flow in the carrier gas.

Typical optical absorption spectrum of SWCNTs exhibited a strong absorption peak at ~200 nm, which was generated by the plasma oscillation of electron cloud. Three typical characteristic absorption peaks corresponded to the first Van Hof singularity (E_{11}^{M}) of metallic SWCNT and the first and second Van Hof singularities (E_{11}^{S}, E_{22}^{S}) of semiconducting SWCNT.[31,32] Moreover, SWCNTs were analyzed through the Raman spectroscopy to obtain the structural information. The corresponding metallic and semiconducting SWCNT excitation regions were identified by the combination of Kataura diagram. As the radial breathing modes under three wavelengths of lasers shown in Fig. 2e–g, both peaks of metallic and semiconducting

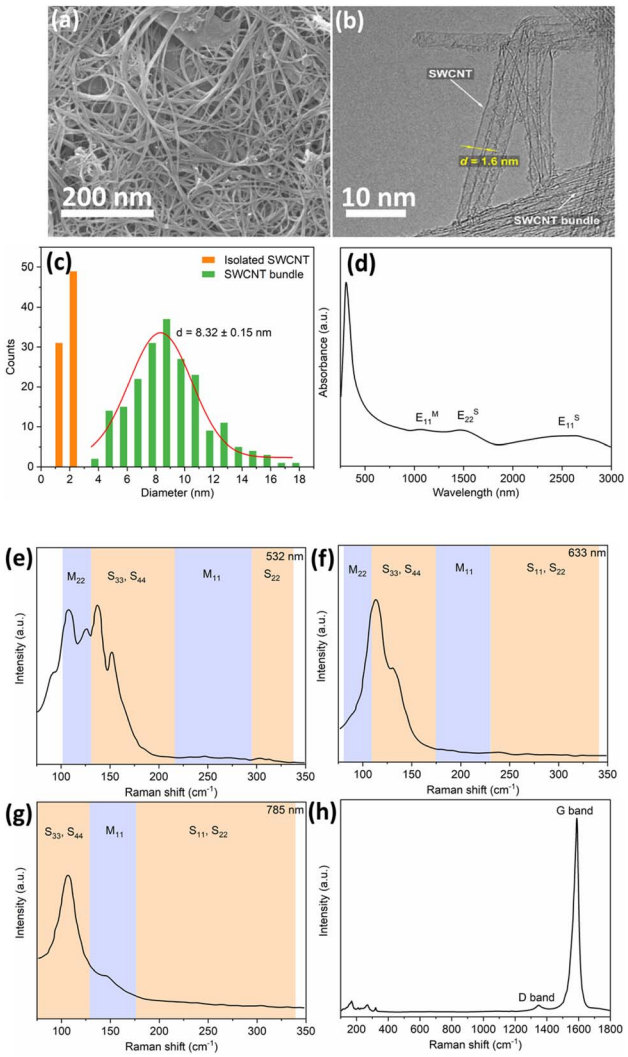

Fig. 2 Characterization results of SWCNTs: (a) SEM image. (b) TEM image. (c) Diameter distribution (c). Optical absorbance of SWCNTs (d). Radial breathing mode excited with the wavelength of 532 nm (e), 633 nm (f) and 785 nm (g). D mode and G mode of SWCNTs (h).

SWCNTs were observed. The average diameter of SWCNTs could be calculated using $d = 248/\delta_{RBM}$ according to the relationship between diameter and respiratory mode. Given the mainly location of breathing mode in 114 cm^{-1}, the corresponding diameter was about 2.2 nm. For carbonaceous materials, intensity ratio of D and G band was commonly applied to investigate the quality of products.[33,34] As shown in Fig. 2h, I_D/I_G value of SWCNTs was as low as 0.058, indicating that the crystallinity was high and defects in products were scare. Taken together, SWCNTs prepared by FCCVD in this work were a mixture of metallic and semiconducting SWCNT, which presented few defects and impurities.

3.2. Characterization of P/SWCNTs/WPU coatings

Poor SWCNTs distribution in polymer because of high diffusion resistance of SWCNTs would induce their agglomeration on granule surface of polymer. Hence, an *in situ* polymerization

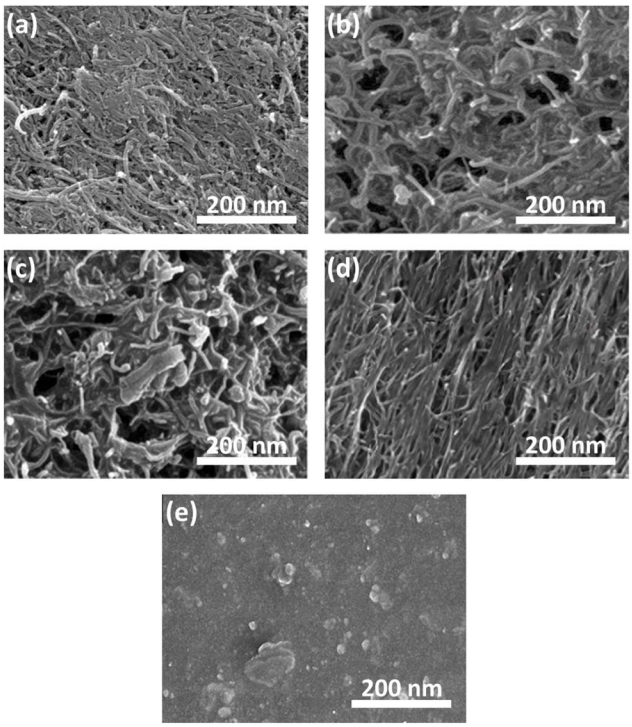

Fig. 3 SEM observation of P/SWCNTs/WPU-1 to -4 (a–d) and WPU (e).

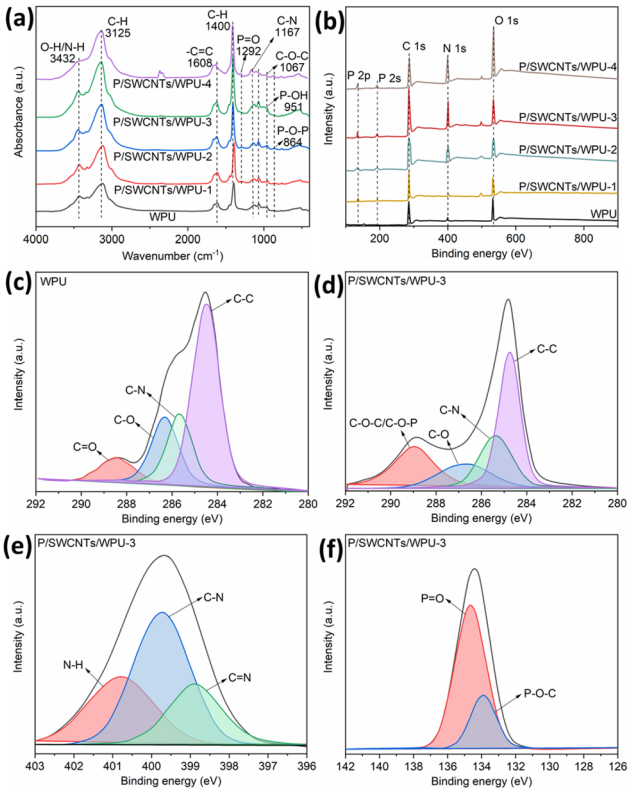

Fig. 4 FTIR (a) and XPS survey spectra (b) of WPU and P/SWCNTs/WPUs. Deconvolution of C 1s of WPU (c) and P/SWCNTs/WPU-3 (d). Deconvolution of N 1s (e) and P 2p (f).

approach was applied in this study to decrease the diffusion resistance given the low molecular weight of organics. The diffusion of SWCNTs in WPU granules could be achieved possibly, benefiting for the formation of electric conductive channel. SWCNTs were uniformly distributed in WPU matrix rather than agglomerated (Fig. 3a–d). Three-dimensional networks derived from the interconnection of SWCNTs would be beneficial for electron and thermal conductivity.

The chemical compositions of WPU and P/SWCNTs/WPUs were analyzed as the FTIR spectra (Fig. 4a). Stretching vibration of O–H/N–H bond located at 3432 cm^{-1}. Stretching vibration of C–H bond at 3125 cm^{-1} and 1400 cm^{-1} were exhibited. Stretching vibration of C=C and C–O–C at 1608 cm^{-1} and 1067 cm^{-1}, were presented. It was worth noting that stretching vibrations of P=O, P–OH and P–O–P were newly emerged at 1292, 951 and 864 cm^{-1}.[35] It is indicated that the phosphorous-containing components have been successfully introduced to WPU matrix.

The chemical states of elements on the surface of WPU and P/SWCNTs/WPU analyzed *via* XPS were illustrated in Fig. 4b–f. C, O, and N were three typical elements existed on the surface of WPU, while C, O, N and P were four typical elements existed on the surface of P/SWCNTs/WPU. For WPU, C 1s could be deconvoluted into four components including C–C at 284.5 eV, C–N at 285.7 eV, C–O at 286.3 eV and C=O at 288.4 eV (shown in Fig. 4c).[36] The atomic ratios of these four species were 56.0%, 19.3%, 16.2% and 8.5%, respectively. For P/SWCNTs/WPU-3, deconvoluted peak at 286.3 eV should be derived from C–O–C and C–O–P (shown in Fig. 4d). C–O–C/C–O–P atomic ratio increased significantly to 26.3%. N 1s of P/SWCNTs/WPU-3 was compose of N–H (400.8 eV), C–N (399.7 eV) and C=N (398.9 eV). While N 1s peak of WPU presented a weak intensity and should be ascribed to the C=N in the matrix of WPU. P 2p of P/SWCNTs/WPU-3 was compose of P=O (134.6 eV) and P–O–C (133.8 eV). Taken together, increasing C–O–C/C–O–P ratio and the emerging covalently bonding of N and P 2p indicated the successful combination of APP and SWCNTs in the matrix of WPU.

3.3. Thermal stability and flame retardancy evaluation

Thermal behaviors of samples in nitrogen atmosphere were investigated *via* TGA and DTA as displayed in Fig. 5. The thermal behaviors of WPU were composed of two period. Specifically, the first stage from 305 °C to 392 °C was derived from the depolymerization of WPU matrix by generating volatile products, aliphatic and aromatic carbon. The second period was derived from the decomposition of aliphatic and aromatic carbon to CO_2. Similar to the thermal decomposition trend of WPU, SWCNTs/WPU presented a high residue mass, demonstrating that SWCNTs had a good charring ability at high temperature. As for P/WPU and P/SWCNTs/WPUs, the decomposition temperature decreased significantly with rising temperature owing to APP decomposition by losing water molecules. Residue contents of samples rose with SWCNT contents in composites. P/SWCNTs/WPU-3 presented the highest residue mass of 30.7%. As the content of SWCNTs

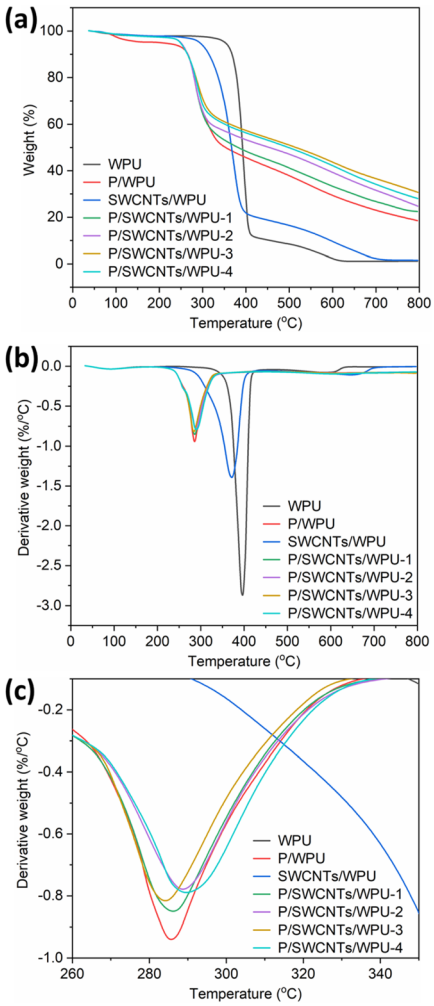

Fig. 5 TGA curves (a) and DTG curves (b and c) of WPU, P/WPU, SWCNTs/WPU, P/SWCNTs/WPUs.

increased further, the residue mass reduced, which should probably due to the poor dispersion of SWCNTs with high content in the matrix of WPU. Volatiles formed and diffused with heat transformation would be hampered by adding SWCNTs and APP. From this observation, it is verified that the thermal stability of WPU could be significantly enhanced through the synergistic integration of APP and SWCNTs. From the TGA analysis, the mass contents of SWCNTs in P/SWCNTs/WPUs were 17.5% for P/SWCNTs/WPU-1, 21.5% for P/SWCNTs/WPU-2, 26.1% for P/SWCNTs/WPU-3, and 29.8% for P/SWCNTs/WPU-4. The thermal conductivity values for P/SWCNTs/WPUs were 3.6 W (m^{-1} K^{-1}) for P/SWCNTs/WPU-1, 5.9 W (m^{-1} K^{-1}) for P/SWCNTs/WPU-2, 7.1 W (m^{-1} K^{-1}) for P/SWCNTs/WPU-3, and 7.3 W (m^{-1} K^{-1}) for P/SWCNTs/WPU-4 as shown in Fig. S1.

The mechanical properties of shielding materials are crucial in practical application. The tensile strengths of the composite films were tested using universal tensile testing machine. As present in Fig. S2, the tensile strengths of P/SWCNTs/WPUs were 26.8 MPa for P/SWCNTs/WPU-1, 23.1 MPa for P/SWCNTs/WPU-2, 19.6 MPa for P/SWCNTs/WPU-3, and 16.4 MPa for P/SWCNTs/WPU-4. With the increase of SWCNTs content, the tensile strength of P/SWCNTs/WPUs gradually decreased, which indicated that excessive SWCNTs would reduce the effective interfacial interaction. The waterproof performance of shielding materials are also important for their practical applications. The waterproof performance of the composite films were evaluated using the contact angle measurement. As present in Fig. S3, the contact angles of P/SWCNTs/WPUs were 128.4° for P/SWCNTs/WPU-1, 124.6° for P/SWCNTs/WPU-2, 118.3° for P/SWCNTs/WPU-3, and 112.5° for P/SWCNTs/WPU-4. With the increase of SWCNTs content, the waterproof performance of P/SWCNTs/WPUs decreased gradually. The surfaces of P/SWCNTs/WPUs were hydrophobic, which was beneficial for the prevention of pollutant attachment.

Flame retardancy performances of samples were evaluated through the vertical flammability and LOI tests. Pure WPU was of high flammability and almost no residue was observed after the vertical burning as shown in Fig. 6a. After the combination with APP/SWCNTs, the damage length decreased significantly to 6.3 cm for P/SWCNTs/WPU-1, 5.8 cm for P/SWCNTs/WPU-2 (Figure 6b), 4.6 cm for P/SWCNTs/WPU-3 (Fig. 6c), and 4.9 cm for P/SWCNTs/WPU-4 (Fig. 6d). As shown in Fig. 6e, LOI values increased gradually, *i.e.*, 17.7% for WPU, and 27.5%, 31.2%, 34.1% and 32.6% for P/SWCNTs/WPU-1 to -4. The original morphologies apart from partial carbonization of P/SWCNTs/WPUs were maintained. P/SWCNTs/WPU-3 and 4 reached UL94 V-0 level and could be distinguished as nonflammable materials.

P/SWCNTs/WPU-3 exhibited a well-preserved morphology except for some shrinkage and gas bubbles. Gas bubbles were produced by the decomposing ammonium polyphosphate and the releasing ammonia. During the combustion process, the

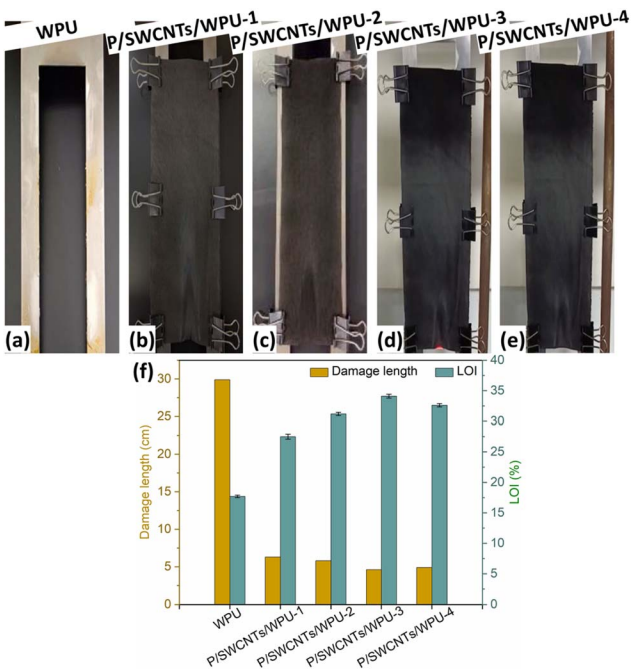

Fig. 6 Illustration for vertical burning test (a). Damage lengths (b–e) and LOI values (f) of WPU and P/SWCNTs/WPUs.

presence of the SWCNTs enhanced the flame retardant efficiency of ammonium polyphosphate, which promoted the dehydration and carbonization process leading to the formation of the char layer and the release of ammonia, water, and carbon dioxide. It is indicated that the unique combination of SWCNTs and ammonium polyphosphate produced a thicker film and formed a more protective layer. Meanwhile the addition of SWCNTs manifested its synergistic flame retardant effect, which promoted the formation of char and reduced the diffusion of heat and oxygen, resulting in the reduction of volatile combustibles. Therefore, the flame retardant mechanism for P/SWCNTs/WPUs was proposed as following. In the initial stage of combustion process, the temperature elevated sharply, and the dehydration condensation reaction occurred between the ammonium polyphosphate and WPU. Simultaneously, WPU molecular chains were pyrolyzed and carbonized. Moreover, the incorporation of SWCNTs promoted the formation of char on the WPU surface. The char layer containing carbon–nitrogen heterocycles provided a barrier effect to inhibit the release of volatile combustibles, such as hydrocarbons, ethers, and carbonyls. As a result, the combustion process became difficult to continue, causing WPU to self-extinguish.

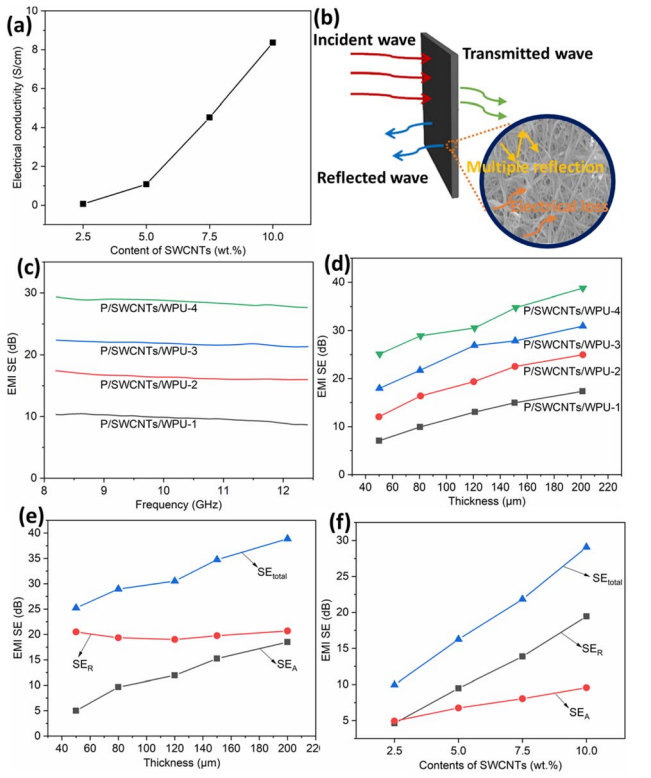

Fig. 7 Electrical conductivity evaluation (a). Schematic illustration of EMI shielding (b). EMI SE of P/SWCNTs/WPU coatings as functions of frequency of 8.2–12.4 GHz (c) and thickness (d). EMI SE parameters of P/SWCNTs/WPU-4 with various thickness at the frequency of 10 GHz (e). EMI SE parameters of P/SWCNTs/WPU with various SWCNT content at the frequency of 10 GHz and thickness of 80 μm (f).

3.4. Electrical conductivity and EMI shielding of P/SWCNTs/WPU coatings

Electric conductivity of P/SWCNTs/WPUs (Fig. 7a) rose as 0.05, 1.08, 4.52 and 8.36 S cm^{-1} for P/SWCNTs/WPU-1 to -4. As illustrated in Fig. 7b, SE was applied to evaluate the EMI capability of materials to attenuate electromagnetic waves emitted from transmitting antenna, which was calculated as $SE = 10 \log(P_0/P_S)$, where P_0 and P_S were the power density of receiving wave in the presence and absence of EMI shielding materials, respectively. Taking the EMI values of P/SWCNTs/WPUs at the frequency of 10 GHz as examples, EMI SE were 9.9 dB (for P/SWCNTs/WPU-1), 16.3 dB (for P/SWCNTs/WPU-2), 21.8 dB (for P/SWCNTs/WPU-3) and 28.7 dB (for P/SWCNTs/WPU-4), showing a rising trend with the rising SWCNT content from 5% to 20%. Since the thickness of evaluated samples plays an important role in EMI, EMI SE values showed a rising tendency with thickness (Fig. 7d). For instance, P/SWCNTs/WPU-4 increased from 25.1 to 38.8 dB with thickness from 50 to 200 μm.

There are two types of EMI mode for electromagnetic waves including reflection (SE_R) and absorption (SE_A). The reflection of electromagnetic waves is attributed to the impedance mismatch of interface between air and material. While the absorption of electromagnetic waves is ascribed to the electrical loss and multiple reflection at the interface between fillers and WPU. SE_R and SE_A values were calculated as $SE_R = -10 \log(1 - S_{11}^2)$ and $SE_A = -10 \log(S_{21}^2/(1 - S_{11}^2))$, where S_{11} and S_{21} were the scattering parameters measured by vector network analyzer. Taking the reflection and absorption of electromagnetic waves at the frequency of 10 GHz for P/SWCNTs/WPU-4 as examples, SE_R of P/SWCNTs/WPU-4 changed slightly which SE_A changed from 5.0 dB to 18.5 dB as the thickness rose from 50 μm to 200 μm (shown in Fig. 7e). Moreover, EMI SE parameters of P/SWCNTs/WPUs with various SWCNT content at the frequency of 10 GHz and thickness of 80 μm were also investigated as shown in Fig. 7f. Both the values of SE_R and SE_A increased with the rising filling content of SWCNTs in P/SWCNTs/WPUs. Notably, the rising trend of SE_R values (4.6–19.3 dB) was more obvious compared with that of SE_A values (4.9–9.6 dB). Given the significantly higher electrical conductivity of P/SWCNTs/WPUs with higher SWCNT content, the enhancement of conductivity played a more essential role for the improvement of SE_R.

Since the EMI durability of materials which are deformed through bending are crucial for their real applications, EMI SE values of P/SWCNTs/WPU-4 were evaluated after 1000 times of bending tests, which were carried out with angle of 180 °C at the frequency of 2 Hz (Fig. 8a). Specifically, EMI SE values before and after 1000 times of bending changed slightly (Fig. 8b), which demonstrated the stable structure of coating during the bending test. The thickness of the sample for EMI durability bending testing was 80 ± 1.4 μm. After 1000 times of bending, electrical conductivity of film decreased with a ratio of 1.8% as displayed in Fig. 8c. From the above observation, P/SWCNTs/WPU coating presented excellent durability of EMI and

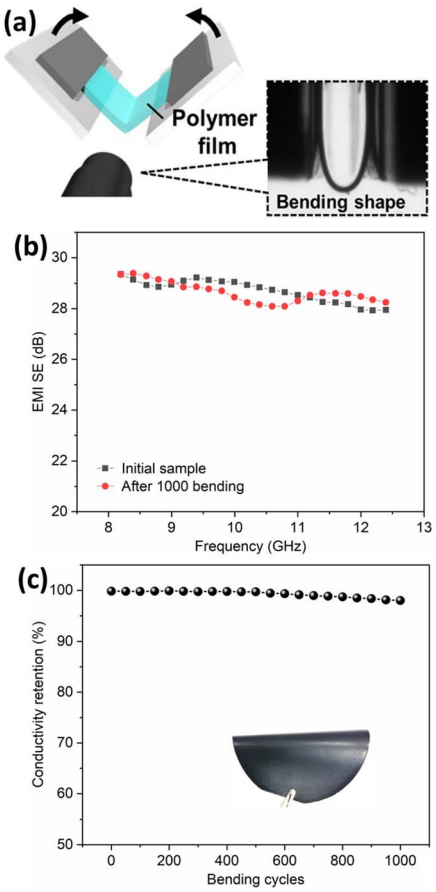

Fig. 8 Schematic for bending test (a). EMI SE before and after 1000 times of bending (b). Retention of electric conductivity changes for 0–1000 times of bending (c).

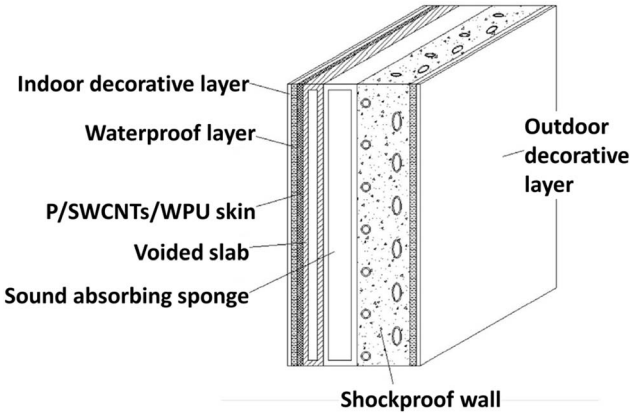

Fig. 9 Design diagram of flame-retardant/EMI shielding wall for buildings.

conductivity, which were especially available in the application of wearable electronics.

A performance comparison of P/SWCNTs/WPUs with other polymer-based EMI shielding materials was provided based on the analysis of EMI SE, thickness (tm), filler loading, and EMI SE/tm as listed in Table S1. P/SWCNTs/WPU-3 with a thickness of 80 μm exhibit a high average EMI SE of 21.8 dB. For comparison, the recent researches on polymer-based EMI shielding composites in the frequency of 8.2–12.4 GHz were listed in Table S1. The EMI SE of P/SWCNTs/WPU-3 is comparable to those of other shielding composites ever reported. Moreover, P/SWCNTs/WPU-3 film presented a higher application potential in this filed due to thin thickness due to the requirement of small size for portable and wearable electronic device.

3.5. Design of flame-retardant/EMI shielding wall for buildings

On the basis of excellent flame-retardant and EMI shielding performances of P/SWCNTs/WPU-3, a flame-retardant/EMI shielding wall was designed using P/SWCNTs/WPU-3. As shown in Fig. 9, a flame-retardant/EMI shielding wall was composed of multiple layers from the sequence from left to right, including an indoor decorative layer, a waterproof layer, P/SWCNTs/WPU-3 layer, a voided slab, a sound-absorbing sponge, a shockproof wall, a waterproof layer and an outdoor decorative layer. The flame-retardant wall for buildings can make the waterproof layer to protect the flame-retardant layer and prevent the water from contacting with the flame-retardant layer. Meanwhile, the sound absorption of the sound-absorbing sponge can be enhanced by arranging the sound-absorbing sponge in the voided slab. The improved sound insulation ability of the wall could increase the privacy of users, making the rest environment quieter and improving the comfort of users.

4 Conclusions

In summary, uniform and clean SWCNTs prepared *via* FCCVD were applied to fabricate novel P/SWCNTs/WPU coating materials through an *in situ* polymerization method. The increasing ratio of C–O–C/C–O–P component and the emerging covalently bonding of N and P 2p indicated the successful combination of APP and SWCNTs in the matrix of WPU. By filling 15 wt% of SWCNTs, P/SWCNTs/WPU-3 exhibited excellent thermal stability and flame retardancy including 4.6 cm of damage length, 34.1% of LOI value and UL94 V-0 level without destroy of original morphology apart from partial carbonization. Moreover, P/SWCNTs/WPU-3 coating presented a superior electrical conductivity (4.52 S cm^{-1}) and EMI shielding effect (21.8 dB). More obvious rising trend of SE_R values (4.6–19.3 dB) than that of SE_A values (4.9–9.6 dB) indicated that the enhancement of conductivity of P/SWCNTs/WPU with higher SWCNT content dominated the improvement of SE_R. Excellent EMI shielding durability with 1.8% of reduced value was achieved after 1000 times of bending, which was derived from the stable structure of coating during the bending test. Herein, an effective guidance for SWCNTs polymer building materials with outstanding flame retardant and EMI was presented.

Author contributions

Junyu Pan: conceptualization, data curation, investigation, methodology, validation, writing-original draft, writing-review & editing. Yang Zhong: conceptualization, methodology, resources.

Conflicts of interest

There are no conflicts to declare.

Data availability

The data that support the findings of this study are available on request from the corresponding author.

Supplementary information contains the results of thermal conductivity values, tensile strengths, contact angles, comparision of EMI performance of P/SWCNTs/WPUs. See DOI: **https://doi.org/10.1039/d5ra05374a**.

Acknowledgements

The supporting characterization of samples from the colleagues of Nano-centre of University of New South Wales was also acknowledged.

Notes and references

1 L. Qi, W. Cai, W. Zhang, B. Wang, W. Li, X. Jin, L. Chen, B. Yu, Y. Hu and W. Xing, *ACS Appl. Mater. Interfaces*, 2023, **15**, 23725–23735.
2 G. D'Agostino, M. R. Caruso, G. Cavallaro, G. Lazzara and S. Milioto, *ACS Appl. Polym. Mater.*, 2024, **6**, 7679–7690.
3 L. Zhang, A. N. Zhang, S. M. He, G. Q. Zheng, F. R. Zeng, Y. Z. Wang, B. W. Liu and H. B. Zhao, *ACS Appl. Mater. Interfaces*, 2024, **16**, 19519–19528.
4 K. Song, X. Bi, C. Yu, Y. T. Pan, H. Vahabi, V. Realinho, J. He and R. Yang, *ACS Appl. Mater. Interfaces*, 2024, **16**, 7617–7630.
5 Q. Jiang, P. Li, Y. Liu and P. Zhu, *J. Colloid Interface Sci.*, 2023, **629**, 392–403.
6 T. T. Huang, K. Ning and B. Zhao, *Int. J. Biol. Macromol.*, 2023, **253**, 126875.
7 W. M. Song, L. Y. Zhang, P. Li, Y. P. Ni and Y. Liu, *Int. J. Biol. Macromol.*, 2024, **260**, 129596.
8 H. Li, D. Wen, S. Wang, Z. Jiang and P. Zhu, *Int. J. Biol. Macromol.*, 2023, **253**, 126812.
9 Y. M. Li, W. J. Hu, S. L. Hu, Y. R. Li and D. Y. Wang, *Chem. Eng. J.*, 2023, **474**, 145803.
10 P. Li, X. C. Jiang, W. M. Song, L. Y. Zhang, Y. J. Xu, Y. Liu and P. Zhu, *J. Cleaner Prod.*, 2023, **411**, 137265.
11 P. Qi, Y. Li, Y. Yao, J. Sun, L. Li, J. Liu, X. Gu, H. Li and S. Zhang, *Chem. Eng. J.*, 2023, **452**, 139453.
12 H. Jia, H. Cui, N. Wu, S. Deng, F. Wang, M. Wang and Z. Wang, *Carbohydr. Polym.*, 2025, **347**, 122540.
13 T. M. Yang and Y. T. Yang, *Int. J. Biol. Macromol.*, 2024, **280**, 136017.
14 X. Zhang, L. Zhang, J. Chen, X. Jiang, Y. Wei, F. Xiao, J. Hu and J. Ding, *Surf. Coat. Technol.*, 2024, **492**, 131201.
15 W. Li, F. Luo and Y. Dai, *Cellulose*, 2024, **24**, 025–9042.
16 T. Cui, Y. Zheng, M. Hu, B. Lin, J. Wang, W. Cai, B. Fei, J. Zhu and Y. Hu, *Small*, 2024, **20**, 2312083.
17 C. Li, W. Wei, L. He, X. Qi, J. He, X. Zhang, X. Han, J. Wang and Z. Gao, *J. Water Process Eng.*, 2024, **65**, 105734.
18 L. Du, Y. Li and P. Zhu, *Surf. Interfaces*, 2024, **50**, 104523.
19 L. F. Guidugli, R. Cheatham, J. Calhoun and M. T. Reza, *Ind. Eng. Chem. Res.*, 2024, **63**, 14811–14820.
20 J. Lu, Y. Zhang, Z. Jiang, Y. Wang, X. Chen, H. Zhang, K. Chen, S. Zhai, Y. Yu and D. Qi, *ACS Sustainable Res. Manage.*, 2024, **1**, 694–706.
21 M. Wu, Y. Chen, H. Y. Yu, X. Liu, Y. Dong, P. C. Qian and X. Wang, *ACS Appl. Nano Mater.*, 2023, **6**, 20866–20877.
22 N. A. Vest, M. O. Convento, D. Rodriguez-Melendez, D. L. Smith, J. R. Ayala, J. A. D. Marquez, M. D. Montemayor, Y. Quan, A. O. Afonso, E. T. Iverson, S. Banerjee, Q. Wang and J. C. Grunlan, *ACS Appl. Eng. Mater.*, 2023, **1**, 3157–3166.
23 Y. Zhang, H. Y. Yu, Y. Dong, X. Wang, X. Chen, X. Ma and P. C. Qian, *ACS Sustainable Chem. Eng.*, 2023, **11**, 12983–12991.
24 V. Duhan, N. Amarnath, S. Yadav and B. Lochab, *ACS Appl. Polym. Mater.*, 2023, **5**, 2971–2982.
25 L. Liu, M. Yao, H. Zhang, Y. Zhang, J. Feng, Z. Fang and P. Song, *ACS Sustainable Chem. Eng.*, 2022, **10**, 16313–16323.
26 F. Liang, Y. Xu, S. Chen, Y. Zhu, Y. Huang, B. Fei and W. Guo, *ACS Appl. Mater. Interfaces*, 2022, **14**, 56027–56045.
27 W. Li, F. Luo, Y. Dai, D. Chen and H. Li, *Cellulose*, 2024, **31**, 9025–9042.
28 B. Manikandan, S. Chakraborty and S. S. Ganesan, *Cellulose*, 2024, **31**, 7189–7206.
29 W. M. Song, L. Y. Zhang, B. H. Wang and Y. Liu, *Polym. Degrad. Stab.*, 2024, **227**, 110863.
30 W. M. Song, L. Y. Zhang, R. Y. Fan, Y. Liu and Y. Z. Wang, *Composites, Part B*, 2024, **287**, 111848.
31 Y. Zhang, L. Tao, L. Zhao, C. Dong, Y. Liu, K. Zhang and H. Liimatainen, *J. Colloid Interface Sci.*, 2024, **676**, 61–71.
32 C. Chen, J. Luan, F. Lan, G. Ji, X. Yin, C. Dong and Z. Lu, *Ind. Crops Prod.*, 2024, **222**, 119623.
33 L. Y. Zhang, W. M. Song, B. H. Wang, P. Li, Y. P. Ni and Y. Liu, *Polym. Degrad. Stab.*, 2024, **228**, 110897.
34 X. Chen, Q. Sun, L. Dun, S. Chen and Y. Wang, *Prog. Org. Coat.*, 2024, **194**, 108617.
35 W. J. Jin, W. L. He, S. S. Cheng, J. P. Guan, X. W. Cheng, R. K. Wu, S. Gaan and G. Q. Chen, *Prog. Org. Coat.*, 2024, **194**, 108563.
36 L. Gao, Y. Bao, P. Tang, C. Liu and W. Zhang, *Cellulose*, 2024, **31**, 8369–8385.